Reduction of Pericyte Coverage Leads to Blood-Brain Barrier Dysfunction Via Endothelial Transcytosis Following Chronic Cerebral Hypoperfusion

Zhengyu Sun
Henan Provincial People's Hospital
Chenhao Gao
Henan Provincial People's Hospital
Dandan Gao
Henan Provincial People's Hospital
Ruihua Sun
Henan Provincial People's Hospital
Wei Li
Henan Provincial People's Hospital
Fengyu Wang
Henan Provincial People's Hospital
Yanliang Wang
Henan Provincial People's Hospital
Huixia Cao
Henan Provincial People's Hospital
Guoyu Zhou
Henan Provincial People's Hospital
Jiewen Zhang
Henan Provincial People's Hospital
Junkui Shang (✉ shangjunkui@yeah.net)
Henan Provincial People's Hospital https://orcid.org/0000-0001-5160-315X

Research

Keywords: cerebral small vessel disease, chronic cerebral hypoperfusion, BBB permeability, pericyte, endothelial transcytosis, white matter lesions, TGF-β signaling

Posted Date: February 9th, 2021

DOI: https://doi.org/10.21203/rs.3.rs-168757/v1

Abstract

Background: Chronic cerebral hypoperfusion (CCH) is the leading cause for cerebral small vessel disease (CSVD). CCH is strongly associated with blood–brain barrier (BBB) dysfunction and white matter lesions (WML) in CSVD. But the effects of CCH on BBB integrity and constituents as well as the cellular and molecular mechanisms about the consequences of BBB dysfunction remain elusive. Whether maintaining BBB integrity can reverse CCH induced brain damage has also not been explored.

Methods: In this study, we used a rat model of CSVD, established via permanent bilateral common carotid artery occlusion (2VO) to mimic the chronic hypoperfusive state of CSVD. The progression of BBB dysfunction and components of the BBB was assessed using immunostaining, western blotting and transmission electron microscopy. Data were analyzed using the one-way ANOVA test or two-tailed unpaired Student's t tests.

Results: We noted a transient yet severe breakdown of the BBB in the CC following CCH. The BBB was severely impaired as early as 1 day post operation and most severely impaired 3 days post operation. BBB breakdown preceded WML and neuroinflammatory responses. Moreover, pericyte loss was associated with BBB impairment and accumulation of serum proteins was mediated by increased endothelial transcytosis in the CC. BBB dysfunction led to brain damage by regulating TGF-β/Smad2 signaling. Further, protection of the BBB via inhibition of endothelial transcytosis ameliorated serum proteins leakage, microglial activation, oligodendrocyte progenitor cells (OPCs) activation and inappropriate TGF-β/Smad2 signaling activation.

Conclusions: Our results indicate that reduced pericyte coverage leads to increased BBB permeability via endothelial transcytosis and protection of the BBB integrity ameliorates brain damage by regulating TGF-β/Smad2 signaling following CCH, therefore reversal of BBB dysfunction may be a promising strategy to treat CSVD.

1. Introduction

Chronic cerebral hypoperfusion (CCH) and blood-brain barrier (BBB) dysfunction are two significant pathology features in aging brain [1–3]. Older age is the single most important risk factor for cerebral small vessel disease (CSVD) [4]. CSVD is one of the most common causes of vascular dementia (VD) [5]. VD is a disease of progressive neurodegeneration that is second only to Alzheimer's disease (AD) in prevalence [6]. CSVD poses serious burden on the development of the society. The pathogenesis of CSVD has not been clearly established. Despite several pathological changes are related to CSVD, including CCH, BBB impairment, oxidative stress, inflammation and white matter hyperintensities (WMH) [7], the cascade of these pathological changes are still not fully understood in CSVD. Therefore, we approached this topic by exploring the cellular and molecular mechanisms that regulate the relationship between CCH and BBB function.

The adult brain relies mostly on continuous influx of glucose from the blood to provide energy. CCH alters brain energy metabolism. Metabolic alterations strongly influence the progression of neurodegenerative processes [8, 9]. CCH is also suggested to be the cause of BBB dysfunction and WMH [10]. By restricting the free diffusion of circulating toxins or pathogens, the BBB provides a homeostatic brain microenvironment for healthy neural function [11, 12]. Cross-sectional studies revealed that CCH is correlated with BBB impairment. CCH is also related to the severity of WMH [10]. BBB impairment is more severe in the proximity of WMH compared to areas of apparently normal WM in CSVD [10, 13]. This indicates that BBB impairment is a key factor linking CCH and WMH in CSVD.

BBB integrity is maintained by endothelial cells (EC), pericytes, astrocytes, microglia, tight junctions (TJ) and extracellular basement membranes (BM) [14]. BBB constituents form a complex, dynamic structure, and BBB impairment therefore involves these many constituents [15, 16]. The precise response of all BBB constituents to CCH has not been thoroughly characterized. Meanwhile, it is also unclear whether BBB breakdown is primary cause or secondary to brain parenchyma damage following CCH. Further, BBB breakdown leads to inflammation, oxidative stress, neural injury, loss of neuronal connectivity and neurodegeneration [17]. Whereas, the molecular mechanisms leading to these consequences after BBB breakdown are still little known following CCH.

The technique of bilateral common carotid artery occlusion (2VO) in rats has been developed in order to mimic the chronic hypoperfusive state of CSVD, and is used as an animal model to probe the mechanisms of CSVD [18]. Based on the evidence presented above, we used the 2VO rat model in this study to determine the effects of CCH on changes in BBB permeability, BBB constituents and brain parenchyma damage. We further explored the molecular mechanisms that regulated neural injury after BBB breakdown and revealed whether BBB impairment was the key pathophysiological mechanism following CCH.

Our results indicate that BBB impairment occurs early in the disease process, preceding neuroinflammatory responses and WML. The mechanism of BBB disruption appears to be pericyte loss. Toxins enter the brain parenchyma through increased endothelial transcytosis after BBB impairment. Protection of BBB integrity via inhibition of endothelial transcytosis alleviates microglial activation, oligodendrocyte progenitor cells (OPCs) activation and inappropriate TGF-β/Smad2 signaling activation. This study helps explain the role of BBB injury following CCH and identifies a new potential therapeutic target to protect BBB integrity, providing a theoretical basis for the formulation of targeted treatment strategies.

2. Material And Methods

2.1. Animals

Adult male Sprague Dawley rats (weighing 280–300 g, aged 8–12 weeks) selected for this study were housed at a temperature of 24–26°C on a 12-hour light/dark cycle with free access to food and water.

Forty-eight rats were used for immunohistochemistry to observe serum proteins leakage and BBB constituent changes in the CC at various time intervals following CCH. Thirty rats were injected with Evans blue (EB) via the tail vein for the assessment of BBB permeability, protein extraction and transmission electron microscopy(TEM). Twelve rats were used to assess BBB protection. All experimental procedures were approved by and performed in accordance with the standards of the Experimental Animal Center of Henan University and Henan Provincial People's Hospital.

2.2. Establishment of CCH model

As previously described [19], CCH of the rats was induced by 2VO. In brief, the surgical procedure was performed under sterile conditions. Rats were anesthetized via intraperitoneal (i.p.) injection of combined ketamine (50 mg/kg) and xylazine (10 mg/kg), and placed in the ventral side up position. A midline incision 2 cm in length was made on the ventral cervical neck region of the rats. Following careful separation of muscle tissue, nerves and other adjacent tissue, the common carotid arteries were identified and permanently closed bilaterally using silk ligation. For the sham operation group, the same procedure exposing the common carotid arteries was duplicated but no ligation was performed. Afterward, the muscle tissue and skin were sutured together in a layered closure. Finally, postoperative rats were placed on a warm blanket to wake.

2.3. Measurement of brain water content and BBB permeability

Brain water content and BBB permeability were examined at 1, 3, 7, and 28 days post operation. EB extravasation was used to assess BBB permeability [20]. In brief, 2% EB (3 mL/kg, Sigma) was injected via the tail vein at various end time points, as mentioned. After 2 h circulation, rats were anesthetized and then perfused transcardially with normal saline solution. Whole brains were collected and divided into left and right hemispheres. Left hemispheres were used for the measurement of brain water content. Right hemispheres were further cut into different sections, 1mm/section, using stainless steel brain matrices for rat (RWD Life Science Inc.). One section was used for Western blotting and one section was used for TEM. Other sections were used for EB extravasation. To measure brain water content, left hemispheres were weighed before and after 24 h oven dehydration at 100 ℃. Wet brain weight/dry brain weight was used to quantify brain water content for statistical analysis. During EB extravasation, sections of right hemispheres were weighed and then homogenized in 1ml of 50% trichloroacetic acid, followed by centrifugation at 10,000 rpm for 30 min. The supernatant was collected and mixed with an equal volume of ethanol. The concentration of EB was determined with spectrophotometry at an absorbance of 620 nm. EB content (μg/g) was calculated according to the standard curve in order to evaluate BBB permeability.

2.4. Histology and immunohistochemistry

At various times post operation, rats were anesthetized and perfused transcardially with 100 ml normal saline solution, followed by 500 ml phosphate-buffered fixative solution with 4% paraformaldehyde (PFA pH 7.4). Next, the brain was removed, post-fixed overnight, and finally cryoprotected in phosphate-

buffered sucrose (30%) for 3–5 days. Frozen sections (20 μm) were prepared using a cryostat (Leica) and processed for histological examination. Immunohistochemistry staining was performed as previously described [21, 22]. The primary antibodies used were: rabbit anti-Olig2 (1:200, Millipore); mouse anti-PCNA (1:200, Invitrogen); rabbit anti-collagen IV (COIV, 1:200, Abcam); chicken anti-albumin (ALB, 1:500, Abcam); mouse anti-IgG (1:200, Jackson ImmunoResearch); mouse anti-PDGFR-β (1:200, Abcam); rabbit anti-desmin (1:100, Cell Signaling Technology); mouse anti-Glut1 (1:200, Abcam); mouse anti-GFAP (1:200, Sigma); rabbit anti-Iba1 (1:300, Wako); rabbit anti-TGF-β1 (1:500, Abcam); rabbit anti-phosphorylated Smad2 (pSmad2, 1:500, Millipore); mouse anti-myelin basic protein (MBP, 1:200, Biolegend); Alexa Fluor 488- and 594-Conjugated Goat Secondary Antibodies (1:500, Thermo Fisher Scientific). Nuclear staining was performed using 4’,6’-diamidino-2-phenylindole dihydrochloride (DAPI, 1:2000, Thermo Fisher Scientific). Sections were examined using a confocal laser scanning microscope (TCS SP8, Leica).

2.5. Western blotting

To determine the change in protein levels in the CC, the CC was isolated from one section closed to bregma 1.0 mm from right hemispheres via fine dissection on ice. Once weighed and the CC tissue was digested in RIPA lysis buffer and homogenized. Protein concentration was quantified and then proteins were separated using 10% SDS–PAGE gels and transferred to nitrocellulose membranes (Invitrogen, USA). After washing three times in TBS with 0.05% Tween-20 (TBST), membranes were blocked in TBST with 5% skim milk for 2 h at room temperature. Membranes were incubated with primary antibodies at 4 ℃ overnight, followed by further incubation with HRP-conjugated secondary antibodies (1:2000) for 1 h at room temperature. Western Bright ECL solution was used to develop bands, which were analyzed using GelPro Analyzer 6.0 software (Media Cybernetics, Rockville, MD, USA).

2.6. TEM

After right hemispheres were divided into 1 mm section, one section closed to bregma 0.0 mm was immediately selected and further cut into 1×1×1 mm tissue blocks. The tissue blocks were incubated with 2.5% glutaraldehyde for 6 h and dehydrated and embedded in epoxy resin. The ultrathin sections were cut at 60 nm thickness and observed under an electron microscope (Hitachi TEM system).

2.7. BBB protection

Imatinib inhibits signaling of tyrosine kinase receptor PDGFR by inducing receptor dimerization via ligand binding of RTK phosphorylation sites [23]. Imatinib has been found to protect BBB integrity [24]. After CCH, rats were administered intraperitoneal (i.p.) injections of imatinib (50 mg/kg) every 12 h for 3 days. The lesion control rats were given normal saline after CCH. After the final injection, six rats were euthanized and perfused.

2.8. Cell number count

To quantify the number of various cell types in the CC, five frame regions were randomly chosen for acquisition of confocal images under a 40× or 63× oil immersion objective with 10–12 μm thick z-stacks

in each section (Leica SP8). Five sections were chosen. Every cell expressing the selected marker was manually counted using Image-Pro Plus 7. Data were presented as average cell number in one frame region per section.

2.9. Quantification of vessel diameter and pericyte coverage

Confocal images were acquired under a 40× objective. Using Image-Pro Plus 7, Glut1-positive vessel diameter was measured manually within a single slice image. Collagen IV-positive brain capillary length and PDGFR-β-positive pericyte length were measured manually using Image-Pro Plus 7. The ratio of PDGFR-β-positive pericyte length to collagen-IV positive brain capillary length was taken to be representative of pericyte coverage.

2.10. Statistical analysis

Multiple group comparisons were performed by one-way ANOVA with Dunnett post hoc test. Two group comparisons was made by two-tailed unpaired Student's t tests. Data normality was assessed using the Shapiro-Wilk test. Data were presented as mean ± SD, using boxplots from max to min. All statistical calculations and graphing were performed using GraphPad Prism 8.0 software. Values were considered significant at $p < 0.05$.

3. Results

3.1. Transient and severe BBB breakdown following CCH

Central nervous system (CNS) homeostasis is dependent on the integrity of the BBB. The BBB prevents dysregulated transit of molecules into the brain and very effectively blocks toxins and pathogens in order to preserve delicate neural functioning [25]. The dynamic changes in BBB integrity and the cascade reaction following CCH are still largely unknown. We began by examining the trend of BBB permeability following CCH. Increased brain water content indicated increased BBB permeability. We found that brain water content was increased 1 day post operation, and the brain edema was most severe 3 days post operation (wet/dry weight ratio: 4.45 ± 0.17, 4.93 ± 0.15 and 5.33 ± 0.19 in Sham, 1 d and 3 d group, respectively) (Fig. 1A, B). Recovery began at 7 days (wet/dry weight ratio: 4.63 ± 0.14 in 7 d group), and brain water content had nearly returned to normal level by 28 days post operation (wet/dry weight ratio: 4.63 ± 0.25 in 28 d group) (Fig. 1B). Measurement of dye leakage following injection of EB into the tail vein was another tool we used to assess BBB integrity. As expected, EB was accumulated in the CC following CCH. EB extravasation was apparent on gross examination of the brain 3 days post operation (Fig. 1A). The trend of accumulation mirrored brain water content (EB concentration: 2.08 ± 1.38, 4.09 ± 1.79, 7.68 ± 1.45, 3.02 ± 1.54 and 2.42 ± 1.89 μg/g in Sham, 1 d, 3 d, 7 d and 28 d group, respectively) (Fig. 1D). These results suggest that severe barrier leakage defects appear as early as 1 day following CCH, and thereafter spontaneous recovery occurs.

After BBB breakdown, endogenous circulating macromolecules leak into the brain, which may be toxic to neuronal function. Using immunostaining, we found significant leakage of the serum protein ALB outside vessels in the CC following CCH. ALB leakage was most severe 3 days post operation (ALB density/Sham: 0.89 ± 0.45, 8.74 ± 4.34, 22.70 ± 5.66, 12.75 ± 4.41 and 2.64 ± 1.16 in Sham, 1 d, 3 d, 7 d and 28 d group, respectively) (Fig. 1C, E). We then examined plasma-derived immunoglobulin G (IgG) deposition in the CC. Using immunostaining, we observed some level of IgG within vessels and some IgG leakage outside vessels (Supplemental Fig. 1A). All IgG was increased at 3 days (all IgG density/Sham: 0.92 ± 0.41, 1.46 ± 0.63, 1.75 ± 0.53, 1.00 ± 0.34 and 1.04 ± 0.38 in Sham, 1 d, 3 d, 7 d and 28 d group, respectively) (Supplemental Fig. 1B). The leaked IgG was significantly increased 1 day post operation, reaching the most severe level at 3 days post operation (outside IgG density/Sham: 2.16 ± 1.16, 7.56 ± 2.21, 29.17 ± 7.60, 5.89 ± 2.26 and 5.19 ± 2.17 in Sham, 1 d, 3 d, 7 d and 28 d group, respectively) (Supplemental Fig. 1C).

3.2. Reduction of pericyte coverage leads to BBB dysfunction following CCH

BBB integrity depends on the totality of BBB structure. We therefore studied the effects of CCH on BBB constituents. Pericytes play an import role in BBB function [24, 26]. Using dual immunostaining for PDGFR-β- and collagen IV-positive brain capillary profiles, we observed the initial changes in pericytes following CCH (Fig. 2). Compared to the sham group, pericyte coverage was significantly decreased 1 day post operation (Fig. 2A). Pericyte coverage loss reached the most severe level 3 days post operation, with a decrease of approximately 65% compared to the sham group (Fig. 2A, C). However, by 7 days post operation, pericyte coverage showed a slight degree of recovery. Recovery reached approximately 84% of coverage of the sham group at 28 days post operation, when pericyte coverage between two groups showed no significant difference (pericyte coverage: 60.13 ± 10.68, 43.81 ± 13.50, 20.97 ± 11.32, 46.12 ± 12.70 and 50.47 ± 19.01 in Sham, 1 d, 3 d, 7 d and 28 d group, respectively) (Fig. 2A, C). By 3 days post operation, capillary length was significantly reduced compared to the sham group (capillary length: 35.41 ± 8.03, 33.09 ± 7.92, 25.93 ± 6.46, 34.70 ± 7.16 and 34.12 ± 8.13 mm in Sham, 1 d, 3 d, 7 d and 28 d group, respectively) (Fig. 2A, B). Correlation analysis found that pericyte coverage was not correlated with capillary length (Fig. 2D), indicating that pericyte coverage loss is not due to capillary length reduction. Western blot analysis also showed that PDGFR-β protein levels decreased from day 1 to day 3 post operation, then increased from days 7 to 28 (Fig. 2E). PDGFR-β protein reduction was most severe 3 days post operation (PDGFR-β/β-actin: 1.24 ± 0.45, 0.67 ± 0.19, 0.17 ± 0.09, 0.57 ± 0.25 and 1.14 ± 0.26 in Sham, 1 d, 3 d, 7 d and 28 d group, respectively) (Fig. 2F). Desmin is another pericyte marker. We sought to further confirm pericyte loss using desmin immunostaining, and the loss pattern was indeed similar to that of PDGFR-β immunostaining (desmin length: 469.7 ± 100.3, 306.0 ± 112.1, 141.3 ± 64.2, 409.9 ± 91.0 and 414.4 ± 124.4 μm in Sham, 1 d, 3 d, 7 d and 28 d group, respectively) (Fig. 3). Interestingly, we found significant negative correlation between pericyte coverage and ALB accumulation (Fig. 3D), indicating that pericyte loss is associated with BBB impairment.

Pericytes are not the only cell type that regulates permeability of the BBB [27]. EC, astrocytes and continuous complexes of endothelial junctions are also integral components of the BBB [28]. To further elucidate the effect of pericyte loss on BBB impairment, we also observed other components of the BBB. Glut1 is a marker of endothelial cells. Using Glut1 immunostaining to observe microvascular changes in the CC, we found no significant reduction in microvascular density (number of capillary: 20.25 ± 4.37, 20.75 ± 3.77, 18.38 ± 4.81, 21.50 ± 5.76 and 22.00 ± 6.09/section in Sham, 1 d, 3 d, 7 d and 28 d group, respectively) and an increase in microvascular diameter (diameter of capillary: 5.58 ± 1.58, 7.19 ± 2.22, 10.44 ± 3.20, 7.55 ± 1.67 and 4.57 ± 1.21 μm in Sham, 1 d, 3 d, 7 d and 28 d group, respectively) (Supplemental Fig. 2). We then examined the expression of complexes between EC according to markers (i.e. occludin and claudin-5) for TJ. The expression of occludin was downregulated 3 days post operation compared to the sham group (occludin/β-actin: 0.57 ± 0.15, 0.47 ± 0.08, 0.34 ± 0.14, 0.50 ± 0.07 and 0.52 ± 0.16 in Sham, 1 d, 3 d, 7 d and 28 d group, respectively). However, there was no significant downregulation of claudin-5 expression following CCH (claudin-5/β-actin: 1.27 ± 0.24, 1.26 ± 0.41, 1.05 ± 0.11, 1.17 ± 0.24 and 1.22 ± 0.22 in Sham, 1 d, 3 d, 7 d and 28 d group, respectively) (Supplemental Fig. 3).

Astrocytic coverage of blood vessels is also vital for BBB integrity [29]. Although the number of GFAP-positive astrocytes was significantly increased (9.25 ± 3.62, 10.13 ± 3.31, 29.25 ± 11.80, 19.75 ± 5.31 and 10.63 ± 3.02 cells/section in Sham, 1 d, 3 d, 7 d and 28 d group, respectively), astrocytic vessel coverage was not increased following CCH (astrocytic coverage(%): 33.21 ± 6.47, 30.87 ± 12.31, 32.79 ± 8.14, 42.60 ± 5.89 and 37.81 ± 6.05 in Sham, 1 d, 3 d, 7 d and 28 d group, respectively) (Supplemental Fig. 4). This indicates that astrocyte activation is intended to increase neuroinflammation, not to promote astrocytic coverage of microvasculature following CCH.

3.3. Neurotoxic molecules across the BBB occur through endothelial transcytosis following CCH

We further used TEM to observe the ultrastructural changes of BBB. We found the microvascular was edema and BM thickness was increased 1 day post operation (BM thickness: 100.20 ± 22.39, 186.50 ± 31.60 and 101.00 ± 17.87 μm in Sham, 1 d and 3 d group, respectively) (Fig. 4A, B). The edema was decreased and BM thickness returned to the normal level, but vesicles density in EC was significantly increased 3 days post operation (number of vesicles: 3.0 ± 1.41, 3.0 ± 1.41 and 7.0 ± 2.37/μm^2 in Sham, 1 d and 3 d group, respectively) (Fig. 4A, C). CCH did not alter the ultrastructure of endothelial TJ (Supplemental Fig. 5). These results indicate that large neurotoxic molecules enter the brain parenchyma through increased endothelial transcytosis.

3.4. BBB dysfunction precedes neuroinflammation and demyelination following CCH

Neuroinflammation is an important factor in the pathogenesis of CSVD [30, 31]. The number of microglia reached its peak 3 days post operation, and 86% were activated microglial cells. From day 7 to 28 post

operation, the number of microglia decreased (7.60 ± 2.86, 11.84 ± 3.24, 41.12 ± 10.69, 14.20 ± 6.31 and 13.52 ± 6.38 cells/section in Sham, 1 d, 3 d, 7 d and 28 d group, respectively). But 58% of microglial cells were still activated at 28 days (percentage of activated microglial: 23.32 ± 6.63, 32.62 ± 12.35, 87.08 ± 9.05, 61.23 ± 17.56 and 59.52 ± 16.07 in Sham, 1 d, 3 d, 7 d and 28 d group, respectively), indicating that neuroinflammation persisted until at least 28 days post operation (Supplemental Fig. 6).

WML is another core pathological change of CSVD [32]. The myelin sheath is formed by mature myelin-producing oligodendrocytes, and WM damage is caused by the loss of mature myelin-producing oligodendrocytes [33]. Using immunohistochemistry staining for MBP, a marker for myelin sheath in neuronal axons, we found the MBP density in CC was progressive decreased from 3 days to 28 days after operation (MBP density/Sham: 0.96 ± 0.10, 0.82 ± 0.14, 0.80 ± 0.12, 0.55 ± 0.12 and 0.58 ± 0.15 in Sham, 1 d, 3 d, 7 d and 28 d group, respectively) (Supplemental Fig. 7A, B). Until 28 days after operation, this downregulation had significantly difference compared with sham group (Supplemental Fig. 7B). WB analysis also showed lower MBP protein levels 28 days post operation (MBP/β-actin: 1.64 ± 0.41, 1.50 ± 0.31, 1.37 ± 0.30, 0.54 ± 0.20 and 0.65 ± 0.22 in Sham, 1 d, 3 d, 7 d and 28 d group, respectively) (Supplemental Fig. 7C, D). Although there was a slight increase of MBP protein level 56 days post operation, it was no significantly difference compared with 28 days. These results indicate that BBB breakdown precedes neuroinflammation and WML, and therefore BBB breakdown may be a key pathological event following CCH.

3.5. BBB dysfunction activates TGF-β signaling following CCH

After traumatic brain injury (TBI), serum protein leakage cause robust injury response by activating the transforming growth factor-β (TGF-β) signaling pathway [34, 35]. Hence, we next investigated whether TGF-β signaling pathway also as a candidate mechanism induced brain injury following CCH (Fig. 5). Immunostaining pSmad2, the downstream of the TGF-β receptors, we found the number of pSmad2-positive cells (102.30 ± 17.55, 120.60 ± 20.55, 145.40 ± 25.78, 123.70 ± 14.21 and 110.70 ± 21.65 cells/section in Sham, 1 d, 3 d, 7 d and 28 d group, respectively) and the pSmad2 density (pSmad2 density/Sham: 1.01 ± 0.20, 1.62 ± 0.56, 5.22 ± 1.64, 3.84 ± 1.10 and 1.88 ± 0.61 in Sham, 1 d, 3 d, 7 d and 28 d group, respectively) were significantly increased 3 days post operation compared with sham group (Fig. 5A-C). Using western blotting, we further found increased concentration of pSmad2 (pSmad2/β-actin(%): 14.03 ± 2.97, 23.50 ± 2.51, 28.26 ± 2.48, 20.85 ± 2.34 and 15.06 ± 2.59 in Sham, 1 d, 3 d, 7 d and 28 d group, respectively) and TGF-β1 (TGF-β1/β-actin(%): 50.13 ± 4.34, 45.40 ± 4.13, 67.15 ± 4.56, 62.10 ± 3.93 and 45.40 ± 7.46 in Sham, 1 d, 3 d, 7 d and 28 d group, respectively) following CCH (Fig. 5D-F). The result indicates that the trend of TGF-β signaling activation is consistent with BBB breakdown. The consequences of BBB breakdown is regulated by TGF-β signaling following CCH.

3.6. Protection BBB integrity ameliorates brain damage following CCH

Neurotoxic molecules entered the brain parenchyma via increased endothelial transcytosis following CCH, we next investigated whether inhibition of endothelial transcytosis could ameliorate brain damage. Imatinib can effectively decreased BBB permeability occurred by endothelial transcytosis [24]. We found that imatinib treatment significantly reduced brain IgG accumulation 3 days post operation (100.00 ± 37.41 and 16.04 ± 7.81 in Saline and Imatinib group) (Fig. 6A, B). This indicates Imatinib shows effectively BBB integrity maintenance following CCH. We further assessed pathological outcomes after Imatinib treatment. We found the number of proliferative OPCs (16.67 ± 6.11 and 9.27 ± 3.63 cells/section in Saline and Imatinib group) and activated microglia (42.96 ± 8.72 and 21.52 ± 7.07 cells/section in Saline and Imatinib group) were decreased after imatinib treatment 3 days post operation (Fig. 6C-E, G). Further, TGF-β signaling was also decreased (126.60 ± 24.03 and 98.11 ± 22.27 cells/section in Saline and Imatinib group) (Fig. 6F, H, I). The results indicate that BBB dysfunction directly involves in the regulation of neuroinflammation responses and OPCs proliferation by regulating TGF-β signaling.

4. Discussion

While it has been found that CCH and BBB dysfunction contributes to the pathology of CSVD [10, 36], it is still poorly understood exactly which BBB component becomes impaired, how neurotoxic molecules are able to enter into the parenchyma, and whether protection of BBB integrity can be used as a treatment strategy in CSVD. WML, in contrast, are well understood to be the hallmark pathology of CSVD [10, 32]. The molecular mechanisms that leading to brain parenchymal damage after BBB breakdown are also yet to be properly examined following CCH. In this study, we observed the timeline of both BBB dysfunction and WML following CCH. We revealed that BBB leakage occurs earlier than other pathological events, including OPCs activation, mature oligodendrocyte loss, astrocytic activation, and microglial activation, following CCH. Meanwhile, we examined the constituents of BBB thoroughly. The key change in the BBB constituents following CCH is pericyte loss, which is apparently the leading cause for BBB impairment. Blood-derived pathogens enter into the brain parenchymal through increased endothelial transcytosis. TGF-β signaling regulates the consequences of BBB breakdown following CCH. Our findings suggest that disease development resulting from CCH unfolds as follows. CCH leads to reduction of pericyte coverage, which induces increased BBB permeability. Following BBB impairment, blood-derived neurotoxic substances enter the brain parenchyma via endothelial endocytosis. Blood-derived neurotoxic substances initiate the inflammatory response, OPCs activation and other pathological events by regulating TGF-β/pSmad2 signaling pathway. Ultimately, homeostasis of oligodendroglial lineage cells is disturbed, resulting in irreversible WML. Together, these findings demonstrate that BBB impairment plays a predominant regulatory role in the occurrence of brain damage following CCH, suggesting that BBB compromise is the primary driving factor leading to progressive neural dysfunction. Reversal of BBB dysfunction may be a promising strategy to treat CSVD.

BBB limits the free diffusion of molecules from blood to parenchymal for maintaining brain microenvironment homeostasis [28, 37]. BBB dysfunction contributes to the pathology of many neurological diseases, including TBI [34], stroke [38], AD [17], aging [39] and CSVD [10]. Recent studies have shown that BBB dysfunction occurs earlier than cognitive impairment in the hippocampus of AD

[40]. BBB dysfunction is an early biomarker of AD [40]. On the other hand, during normal aging, WM integrity is still maintained after BBB impairment [41]. These results suggest that BBB dysfunction appears in the early stage of neurological diseases, and BBB impairment is the key factor leading to brain parenchymal injury. In this study, we find BBB impairment precedes a series of pathological events, including astrocyte activation, microglia activation, OPCs activation and WML. BBB dysfunction is the link between the blood-derived pathogens and neural dysfunction.

The cellular constituents of BBB include EC and pericyte [28]. It has been reported that EC dysfunction is the primary cause of BBB dysfunction in stroke-prone spontaneously hypertensive rat [42]. This rat model is known to be a model of human sporadic CSVD [43]. On the other hand, Ding et al. analyzed frontal WM post-mortem brains from 124 subjects with post-stroke dementia (PSD), VD, AD, AD-VD (Mixed), and post-stroke non-demented (PSND) stroke survivors as well as normal ageing controls [44]. Ding et al. finds capillary pericyte loss is the common characteristic of these patients [44]. Ding et al. findings indicate that capillary pericyte loss is the structural basis of BBB dysfunction in the aging-related dementias [44]. Furthermore, Bell et al. also finds pericyte control key neurovascular function in the adult brain and during normal aging [45]. Our study find that CCH does not alter microvascular number, endothelial TJ. While microvascular length, occludin protein, pericyte coverage is reduced and microvascular diameter, BM thickness is increased after CCH. Pericyte loss may be the leading cause for BBB impairment and other structural changes may be secondary to pericyte loss after CCH. First, there is a strong positive correlation between pericyte loss and BBB permeability. Second, significant loss of pericytes occurs from 1 days post operation, the early stage of CCH. Most of other structural changes occurs from 3 days post operation. Third, it has reported that pericytes play a critical role in maintaining BBB integrity [24, 26]. Therefore, in combination with other studies and our study, we can infer that the structural basis of BBB impairment shows some common characteristics in a variety of neurodegenerative diseases. This has important implications for development new therapeutic strategies.

EC acts as an important component of direct communication between the blood and the brain parenchyma. EC exhibits two distinctive features in maintaining BBB integrity [25]. One is specialized TJ that blocks paracellular passage between the blood and the brain parenchyma [11]. The other is exhibited unusually low levels of transcytotic vesicles that limits transcellular transport [46, 47]. Our results show that TJ is not damaged and endothelial endocytosis is increased following CCH. This indicates that blood-derived pathogens enter the brain parenchyma through increased endothelial endocytosis after pericyte loss. It is consistent with the results in previous research. Using many adult viable pericyte loss model, Armulik et al. also finds pericyte maintains BBB integrity via a transcytosis route [24].

Although little is known about the regulatory pathways that trigger brain parenchymal injury after BBB breakdown in CSVD, the relevant molecular mechanisms that regulate brain damage in other BBB dysfunction neurological diseases can provide some clues. The interaction between blood-derived proteins and neural structure are mostly studied in AD [17], TBI [35] and aging [39]. TGF-β signaling pathway regulates progressive neural dysfunction after BBB breakdown in TBI and aging [35, 39]. However, the brain region of interest was not focused on CC in TBI and aging. TBI and aging also have

different pathology [48]. However, although the triggers of the mouse model of stroke, multiple sclerosis, TBI and seizure are different, they all have profound BBB disruption [49]. Interestingly, EC RNA-sequencing finds similar gene expression changes of EC in four diseases [49]. We then examine whether TGF-β signaling pathway is the candidate mechanism leading to brain damage following CCH. We find TGF-β/pSmad2 signaling also is upregulated after BBB breakdown following CCH. TGF-β/pSmad2 signaling upregulation is responsible for brain damage. Reversal of BBB dysfunction ameliorates TGF-β/pSmad2 signaling activation and brain damage. Therefore, TGF-β/pSmad2 signaling pathway regulates the brain parenchymal injury after BBB breakdown following CCH. These studies also suggest that although BBB dysfunction has disparate triggers in multiple neurological disorders, the regulatory pathways leading to neurovascular dysfunction after BBB breakdown have similar responses.

It should be noted that although our findings suggest that reduction of pericyte coverage leads to BBB dysfunction through increased endothelial transcytosis following CCH, we cannot answer the question that why EC, directly links the blood and neural function, is not the primary cause of BBB dysfunction [50]. However, BBB dysfunction is related to EC transcytosis after pericyte loss following CCH. Therefore, pericyte and EC are closely linked in BBB function. In the future study, we plan to isolate the brain microvessels fragments from the CC, then generate single-cell suspensions for single-cell RNA sequencing. Further, we use single-cell analysis to study the cause of pericyte loss, the response of EC after pericyte loss and the crosstalk between pericyte and EC. Ultimately, we analyze the relationship between pericyte and EC in health and disease conditions.

5. Conclusions

In summary, our findings show that pericyte regulates BBB permeability and the formation of WML following CCH. We find that loss of pericyte coverage leads to BBB dysfunction and accumulation of neurotoxic molecules. Neurotoxic molecules enter into brain parenchyma via endothelial endocytosis. BBB dysfunction triggers neuroinflammation and other pathological events, leading to increased OPCs proliferation, reduced OPCs maturation and, eventually, the death of mature oligodendrocytes and development of WML. BBB protection ameliorates neurotoxic molecules accumulation and decreases OPCs activation. Thus, our findings have important implications for understanding the pathogenesis of CSVD, and suggest that loss of pericyte coverage is a key trigger. With these insights, potential therapeutic targets can be developed for CSVD.

Abbreviations

2VO: permanent bilateral common carotid artery occlusion; AD: Alzheimer’s disease; ALB: albumin; BBB: Blood–brain barrier; BM: basement membrane; CC: corpus callosum; CCH: chronic cerebral hypoperfusion; CNS: central nervous system; CSVD: cerebral small vessel disease; EB: Evans blue; EC: endothelial cells; MBP: myelin basic protein; OPCs: oligodendrocyte progenitor cells; PSD: post-stroke dementia; PSND: post-stroke non-demented; TBI: traumatic brain injury; TEM: transmission electron

microscopy; TGF-β: transforming growth factor-β; TJ: tight junctions; VD: vascular dementia; WMH: white matter hyperintensities; WML: white matter lesions.

Declarations

Acknowledgements

We thank Henan Provincial Key Laboratory of Kidney Disease and Immunology, Henan Provincial People's Hospital, Zhengzhou University People's Hospital and School of Public Health, Zhengzhou University for technical assistance and data processing.

Author contribution

J.K. Shang, Z.Y. Sun, J.W. Zhang designed the study. Z.Y. Sun, C.H. Gao, D.D. Gao, R.H. Sun, W. Li, F.Y. Wang carried out experiments and tissue staining. Y.L. Wang, H.X. Cao performed tissue imaging. G.Y. Zhou performed data analysis. J.K. Shang wrote the manuscript. All authors read and approved the final manuscript.

Funding

This work was supported by National Natural Science Foundation of China (Grants 81671068, 81873727); China Postdoctoral Science Foundation (Grants 2020M682302); Key Science and Technology Program of Henan Province, China (Grants 201701020, 20210231008).

Availability of data and materials

All data generated and analyzed during the study are included in this published article.

Ethics approval and consent to participate

Rats were used in accordance with the guidelines of Experimental Animal Center of Henan University.

Consent for publication

Not applicable.

Competing interests

The authors declare no competing financial interests.

References

1. Tarumi T, Zhang R. Cerebral blood flow in normal aging adults: cardiovascular determinants, clinical implications, and aerobic fitness. J Neurochem. 2018;144(5):595–608.

2. Pluvinage JV, Wyss-Coray T. Systemic factors as mediators of brain homeostasis, ageing and neurodegeneration. Nat Rev Neurosci. 2020;21(2):93–102.
3. Brady M, Rahman A, Combs A, Venkatraman C, Kasper RT, McQuaid C, et al. Cerebrospinal fluid drainage kinetics across the cribriform plate are reduced with aging. Fluids and Barriers of the CNS. 2020; 17(1).
4. Pantoni L. Cerebral small vessel disease: from pathogenesis and clinical characteristics to therapeutic challenges. Lancet Neurol. 2010;9(7):689–701.
5. Wardlaw JM, Smith C, Dichgans M. Small vessel disease: mechanisms and clinical implications. Lancet Neurol. 2019;18(7):684–96.
6. Dichgans M, Leys D. Vascular Cognitive Impairment. Circ Res. 2017;120(3):573–91.
7. Wardlaw JM, Smith C, Dichgans M. Mechanisms of sporadic cerebral small vessel disease: insights from neuroimaging. Lancet Neurol. 2013;12(5):483–97.
8. Sweeney MD, Kisler K, Montagne A, Toga AW, Zlokovic BV. The role of brain vasculature in neurodegenerative disorders. Nat Neurosci. 2018;21(10):1318–31.
9. Camandola S, Mattson MP. Brain metabolism in health, aging, and neurodegeneration. EMBO J. 2017;36(11):1474–92.
10. Wong SM, Jansen JFA, Zhang CE, Hoff EI, Staals J, van Oostenbrugge RJ, et al. Blood-brain barrier impairment and hypoperfusion are linked in cerebral small vessel disease. Neurology. 2019;92(15):e1669-e77.
11. Profaci CP, Munji RN, Pulido RS, Daneman R. The blood-brain barrier in health and disease: Important unanswered questions. J Exp Med. 2020; 217(4).
12. Kadry H, Noorani B, Cucullo L. A blood-brain barrier overview on structure, function, impairment, and biomarkers of integrity. Fluids Barriers CNS. 2020;17(1):69.
13. Zhang CE, Wong SM, Uiterwijk R, Backes WH, Jansen JFA, Jeukens C, et al. Blood-brain barrier leakage in relation to white matter hyperintensity volume and cognition in small vessel disease and normal aging. Brain Imaging Behav. 2019;13(2):389–95.
14. Kaplan L, Chow BW, Gu C. Neuronal regulation of the blood-brain barrier and neurovascular coupling. Nat Rev Neurosci. 2020;21(8):416–32.
15. Keaney J, Campbell M. The dynamic blood-brain barrier. Febs j. 2015;282(21):4067–79.
16. Abbott NJ, Patabendige AA, Dolman DE, Yusof SR, Begley DJ. Structure and function of the blood-brain barrier. Neurobiol Dis. 2010;37(1):13–25.
17. Merlini M, Rafalski VA, Rios Coronado PE, Gill TM, Ellisman M, Muthukumar G, et al. Fibrinogen Induces Microglia-Mediated Spine Elimination and Cognitive Impairment in an Alzheimer's Disease Model. Neuron. 2019;101(6):1099–108. e6.
18. Farkas E, Luiten PG, Bari F. Permanent, bilateral common carotid artery occlusion in the rat: a model for chronic cerebral hypoperfusion-related neurodegenerative diseases. Brain Res Rev. 2007;54(1):162–80.

19. Niu HM, Ma DL, Wang MY, Chen XP, Zhang L, Li YL, et al. Epimedium flavonoids protect neurons and synapses in the brain via activating NRG1/ErbB4 and BDNF/Fyn signaling pathways in a chronic cerebral hypoperfusion rat model. Brain Res Bull. 2020;162:132–40.
20. Duarte Lobo D, Nobre RJ, Oliveira Miranda C, Pereira D, Castelhano J, Sereno J, et al. The blood-brain barrier is disrupted in Machado-Joseph disease/spinocerebellar ataxia type 3: evidence from transgenic mice and human post-mortem samples. Acta Neuropathologica Communications. 2020;8(1):152.
21. Hao P, Duan H, Hao F, Chen L, Sun M, Fan KS, et al. Neural repair by NT3-chitosan via enhancement of endogenous neurogenesis after adult focal aspiration brain injury. Biomaterials. 2017;140:88–102.
22. Rao JS, Zhao C, Zhang A, Duan H, Hao P, Wei RH, et al. NT3-chitosan enables de novo regeneration and functional recovery in monkeys after spinal cord injury. Proc Natl Acad Sci U S A. 2018;115(24):E5595-E604.
23. Kjell J, Olson L. Repositioning imatinib for spinal cord injury. Neural Regen Res. 2015;10(10):1591–3.
24. Armulik A, Genove G, Mae M, Nisancioglu MH, Wallgard E, Niaudet C, et al. Pericytes regulate the blood-brain barrier. Nature. 2010;468(7323):557–61.
25. Ayloo S, Gu C. Transcytosis at the blood-brain barrier. Curr Opin Neurobiol. 2019;57:32–8.
26. Daneman R, Zhou L, Kebede AA, Barres BA. Pericytes are required for blood-brain barrier integrity during embryogenesis. Nature. 2010;468(7323):562–6.
27. Siegenthaler JA, Sohet F, Daneman R. 'Sealing off the CNS': cellular and molecular regulation of blood-brain barriergenesis. Curr Opin Neurobiol. 2013;23(6):1057–64.
28. Chow BW, Gu C. The molecular constituents of the blood-brain barrier. Trends Neurosci. 2015;38(10):598–608.
29. Alvarez JI, Katayama T, Prat A. Glial influence on the blood brain barrier. Glia. 2013;61(12):1939–58.
30. Qin W, Li J, Zhu R, Gao S, Fan J, Xia M, et al. Melatonin protects blood-brain barrier integrity and permeability by inhibiting matrix metalloproteinase-9 via the NOTCH3/NF-κB pathway. Aging. 2019;11(23):11391–415.
31. Kaiser D, Weise G, Möller K, Scheibe J, Pösel C, Baasch S, et al. Spontaneous white matter damage, cognitive decline and neuroinflammation in middle-aged hypertensive rats: an animal model of early-stage cerebral small vessel disease. Acta Neuropathol Commun. 2014;2:169.
32. Ter Telgte A, van Leijsen EMC, Wiegertjes K, Klijn CJM, Tuladhar AM, de Leeuw FE. Cerebral small vessel disease: from a focal to a global perspective. Nat Rev Neurol. 2018;14(7):387–98.
33. Franklin RJM, Ffrench-Constant C. Regenerating CNS myelin - from mechanisms to experimental medicines. Nat Rev Neurosci. 2017;18(12):753–69.
34. Hay JR, Johnson VE, Young AM, Smith DH, Stewart W. Blood-Brain Barrier Disruption Is an Early Event That May Persist for Many Years After Traumatic Brain Injury in Humans. J Neuropathol Exp Neurol. 2015;74(12):1147–57.

35. Schachtrup C, Ryu JK, Helmrick MJ, Vagena E, Galanakis DK, Degen JL, et al. Fibrinogen triggers astrocyte scar formation by promoting the availability of active TGF-beta after vascular damage. J Neurosci. 2010;30(17):5843–54.
36. Zhang CE, Wong SM, van de Haar HJ, Staals J, Jansen JF, Jeukens CR, et al. Blood-brain barrier leakage is more widespread in patients with cerebral small vessel disease. Neurology. 2017;88(5):426–32.
37. Blanchette M, Daneman R. Formation and maintenance of the BBB. Mech Dev. 2015; 138 Pt 1:8–16.
38. Yang Y, Rosenberg GA. Blood-brain barrier breakdown in acute and chronic cerebrovascular disease. Stroke. 2011;42(11):3323–8.
39. Senatorov VV, Friedman AR, Milikovsky DZ, Ofer J, Saar-Ashkenazy R, Charbash A, et al. Blood-brain barrier dysfunction in aging induces hyperactivation of TGFβ signaling and chronic yet reversible neural dysfunction. Sci Transl Med. 2019;11(521):eaaw8283.
40. Nation DA, Sweeney MD, Montagne A, Sagare AP, D'Orazio LM, Pachicano M, et al. Blood-brain barrier breakdown is an early biomarker of human cognitive dysfunction. Nat Med. 2019;25(2):270–6.
41. Montagne A, Barnes SR, Sweeney MD, Halliday MR, Sagare AP, Zhao Z, et al. Blood-brain barrier breakdown in the aging human hippocampus. Neuron. 2015;85(2):296–302.
42. Rajani RM, Quick S, Ruigrok SR, Graham D, Harris SE, Verhaaren BFJ, et al. Reversal of endothelial dysfunction reduces white matter vulnerability in cerebral small vessel disease in rats. Sci Transl Med. 2018;10(448):eaam9507.
43. Bailey EL, Smith C, Sudlow CL, Wardlaw JM. Is the spontaneously hypertensive stroke prone rat a pertinent model of sub cortical ischemic stroke? A systematic review. Int J Stroke. 2011;6(5):434–44.
44. Ding R, Hase Y, Ameen-Ali KE, Ndung'u M, Stevenson W, Barsby J, et al. Loss of capillary pericytes and the blood-brain barrier in white matter in poststroke and vascular dementias and Alzheimer's disease. Brain Pathol. 2020;30(6):1087–101.
45. Bell RD, Winkler EA, Sagare AP, Singh I, LaRue B, Deane R, et al. Pericytes control key neurovascular functions and neuronal phenotype in the adult brain and during brain aging. Neuron. 2010;68(3):409–27.
46. Ben-Zvi A, Lacoste B, Kur E, Andreone BJ, Mayshar Y, Yan H, et al. Mfsd2a is critical for the formation and function of the blood-brain barrier. Nature. 2014;509(7501):507–11.
47. Andreone BJ, Chow BW, Tata A, Lacoste B, Ben-Zvi A, Bullock K, et al. Blood-Brain Barrier Permeability Is Regulated by Lipid Transport-Dependent Suppression of Caveolae-Mediated Transcytosis. Neuron. 2017;94(3):581–94. e5.
48. Uzunalli G, Herr S, Dieterly AM, Shi R, Lyle LT. Structural disruption of the blood-brain barrier in repetitive primary blast injury. Fluids Barriers CNS. 2021;18(1):2.
49. Munji RN, Soung AL, Weiner GA, Sohet F, Semple BD, Trivedi A, et al. Profiling the mouse brain endothelial transcriptome in health and disease models reveals a core blood-brain barrier dysfunction module. Nat Neurosci. 2019;22(11):1892–902.

50. Chen MB, Yang AC, Yousef H, Lee D, Chen W, Schaum N, et al. Brain Endothelial Cells Are Exquisite Sensors of Age-Related Circulatory Cues. Cell Rep. 2020; 30(13):4418–32 e4.

Figures

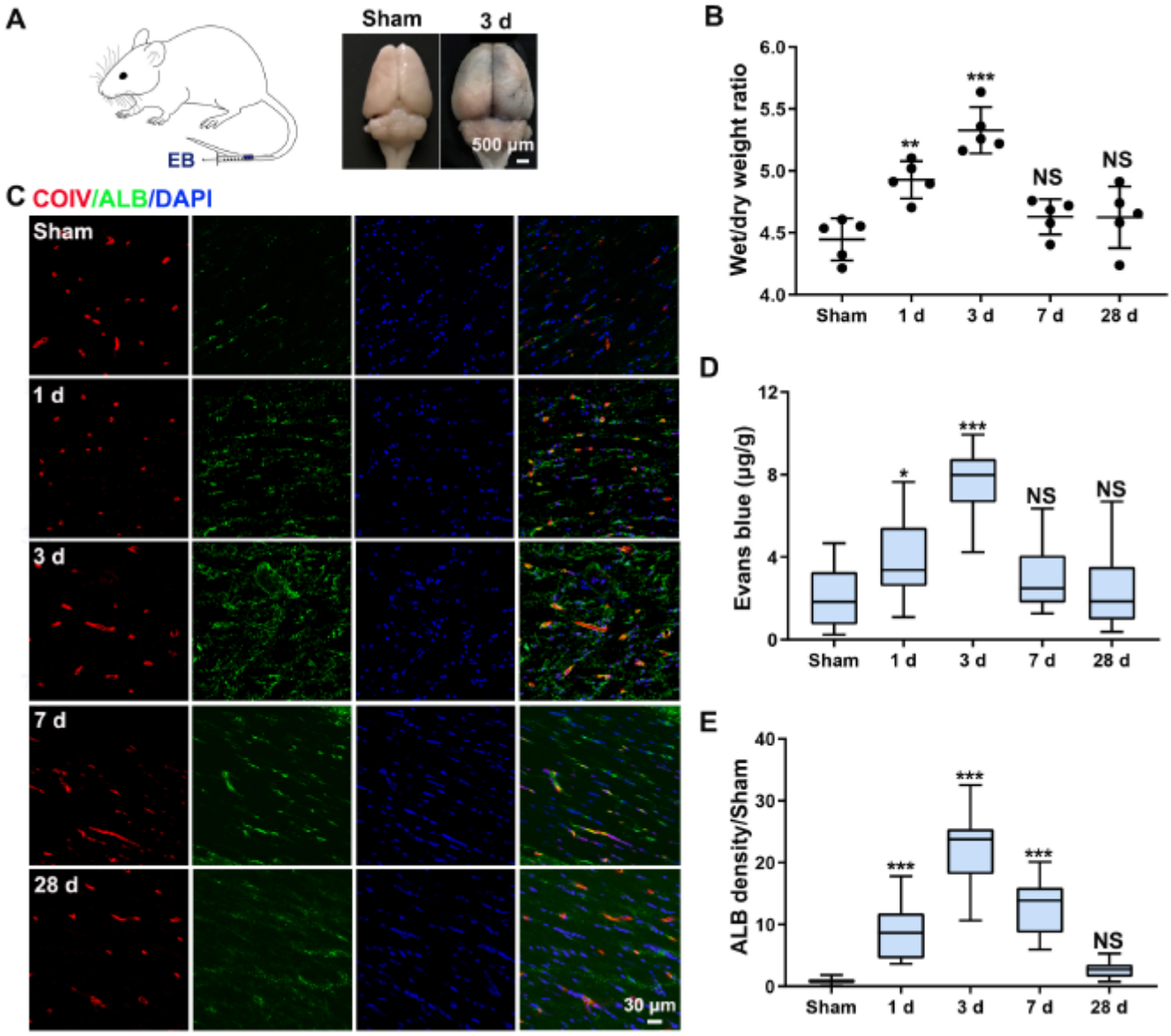

Figure 1

Increased BBB permeability following CCH. (A) Left: schematic illustrating injection of EB into vein; Right: gross anatomic changes in sham group and experimental group 3 days post EB injection. (B) Timeline of brain wet/dry weight ratios post operation. (C) Triple staining for COIV (red), ALB (green) and DAPI (blue) in order to observe ALB leakage in the CC. (D and E) Quantification of Evans blue and ALB at various time points post operation. n=5 per group; NS not significant, *p < 0.05, **p < 0.01, ***p < 0.001; compared to sham group by one-way ANOVA with Dunnett post hoc test.

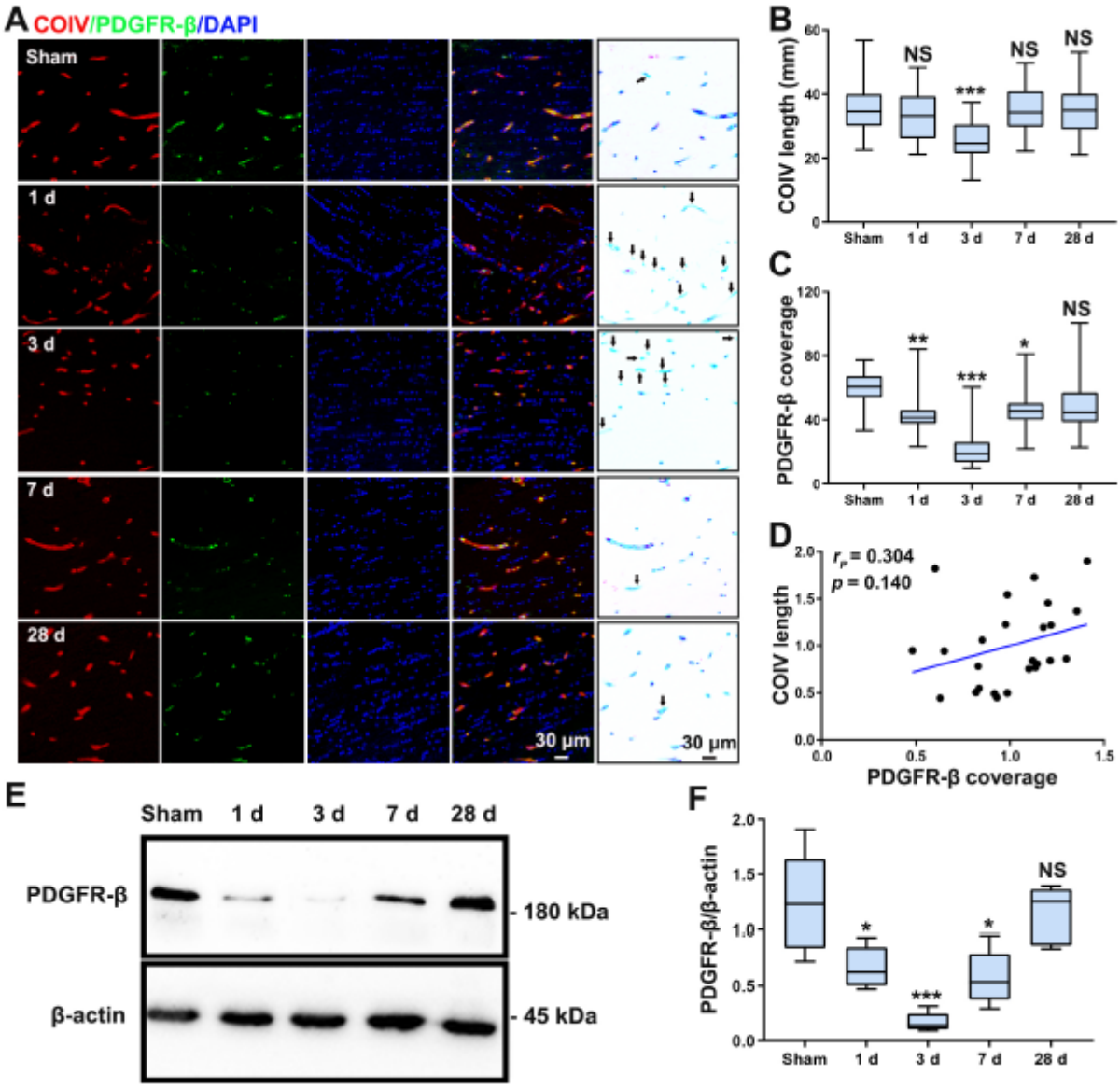

Figure 2

Pericyte loss in the CC following CCH. (A) Triple staining for COIV (red), PDGFR-β (green) and DAPI (blue) in order to observe pericyte coverage of brain capillaries in the CC. Schematic diagram of pericyte coverage loss in capillaries as seen in representative confocal microscopy image is shown in the right column. Black arrows indicate pericyte coverage loss. (B and C) Quantification of COIV-positive capillary length and pericyte coverage in the CC at various time points post operation. (D) Correlation between capillary length and loss of pericyte coverage in the CC at 3 days post operation. (E and F) Western blot and quantification of PDGFR-β expression in the CC at various time points post operation. n=8 per group; NS not significant, *p < 0.05, **p < 0.01, ***p < 0.001; compared to sham group by one-way ANOVA with Dunnett post hoc test.

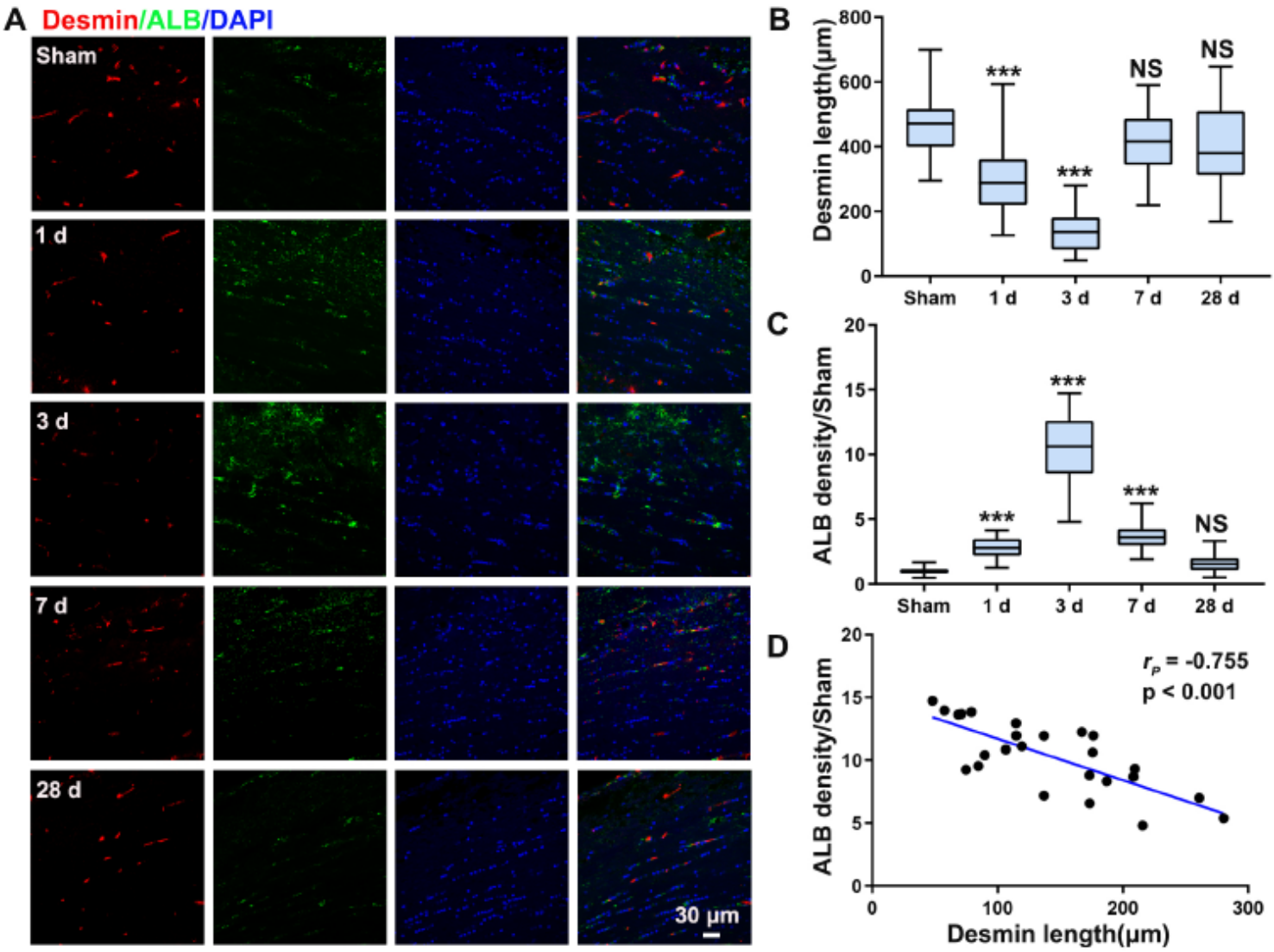

Figure 3

Correlation of pericyte loss and BBB leakage in the CC following CCH. (A) Triple staining for desmin (red), ALB (green) and DAPI (blue) in order to observe the relationship between pericyte loss and BBB impairment in the CC following CCH. (B-C) Quantification of desmin-positive capillary length and ALB density in the CC at various time points post operation. (D) Correlation analysis of pericyte length and ALB density in the CC at 3 days post operation. n=8 per group; NS not significant, ***p < 0.001; compared to sham group by one-way ANOVA with Dunnett post hoc test.

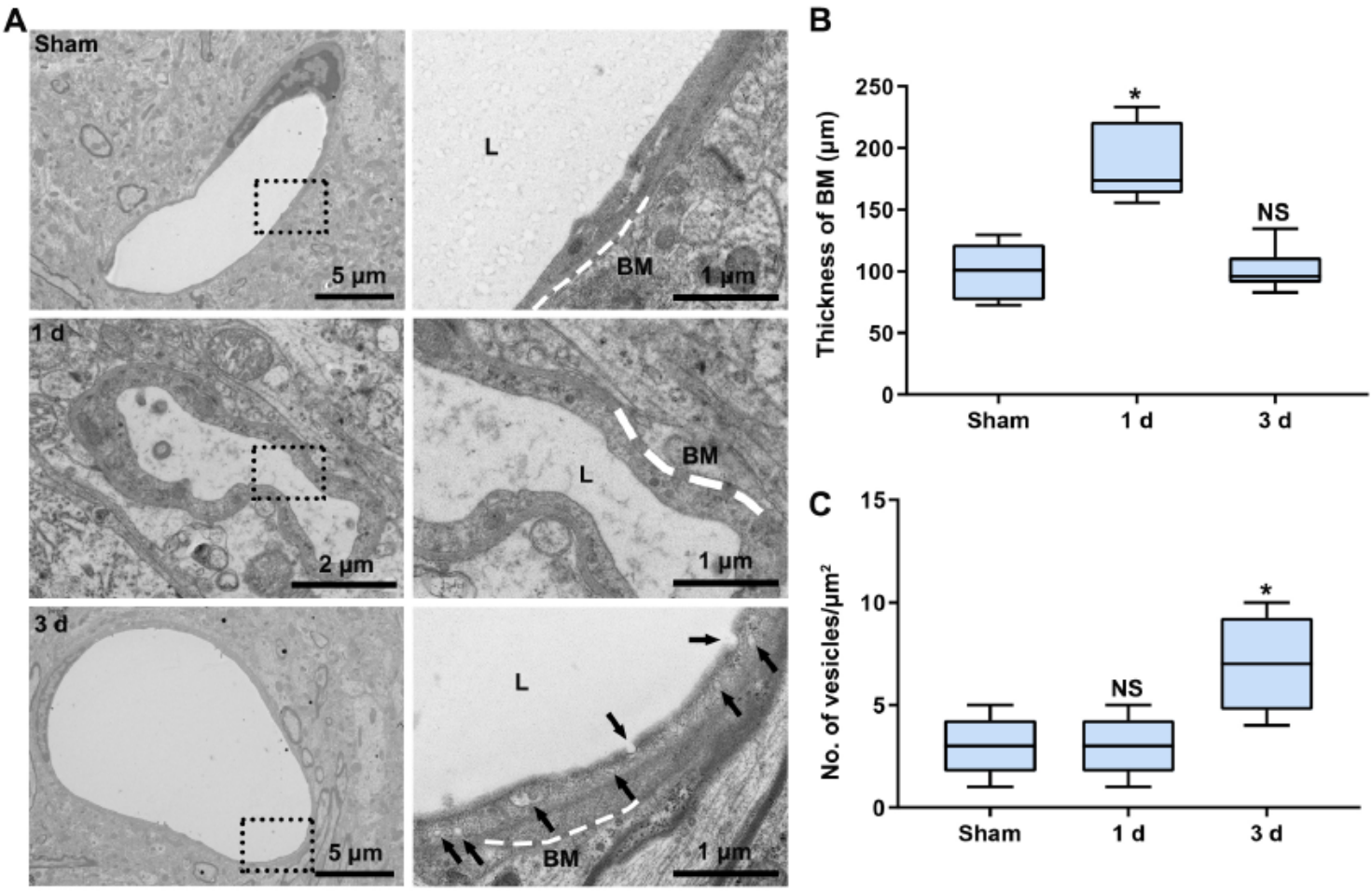

Figure 4

Increased endothelial transcytosis following CCH. (A) Representative images of the ultrastructure of microvascular 1 and 3 days post operation. White dotted lines indicate BM of the vessel. Black arrows indicate vesicles in endothelial cells. (B and C) Quantification of the thickness of BM and the number of vesicles in endothelial cells. n=5 per group; NS not significant, *p < 0.05; compared to sham group by one-way ANOVA with Dunnett post hoc test.

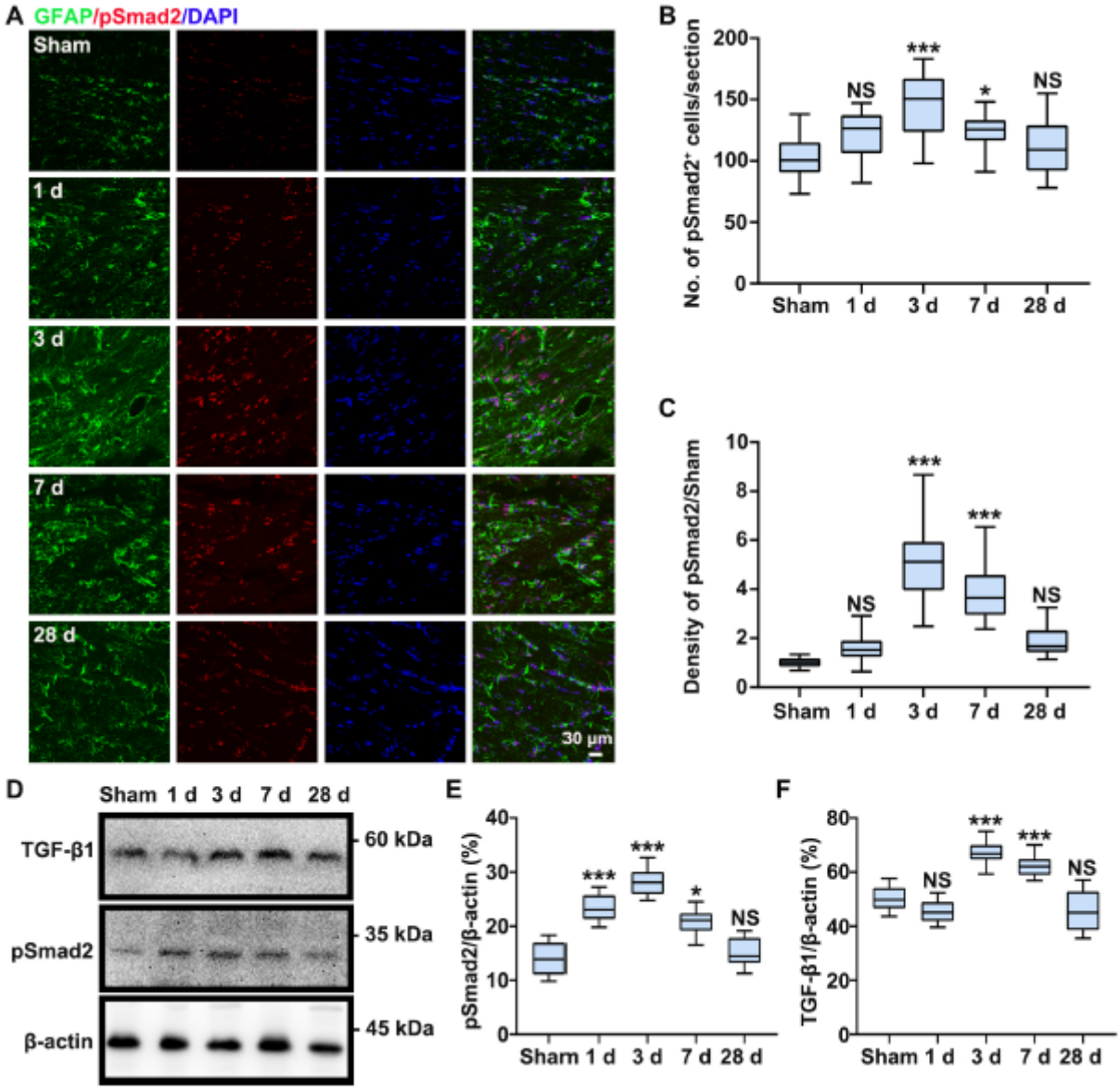

Figure 5

Activation of TGF-β signaling after BBB breakdown following CCH. (A) Immunofluorescence staining of GFAP and pSmad2 at various time points post operation. (B and C) Quantification of pSmad2+ cells and pSmad2 density in the CC at different time points after operation. (D-F) Western blot and quantification of pSmad2 and TGF-β1 expression in the CC at different time points after operation. n=5 per group; NS not significant, *p < 0.05, ***p < 0.001 compared to sham group by one-way ANOVA with Dunnett post hoc test.

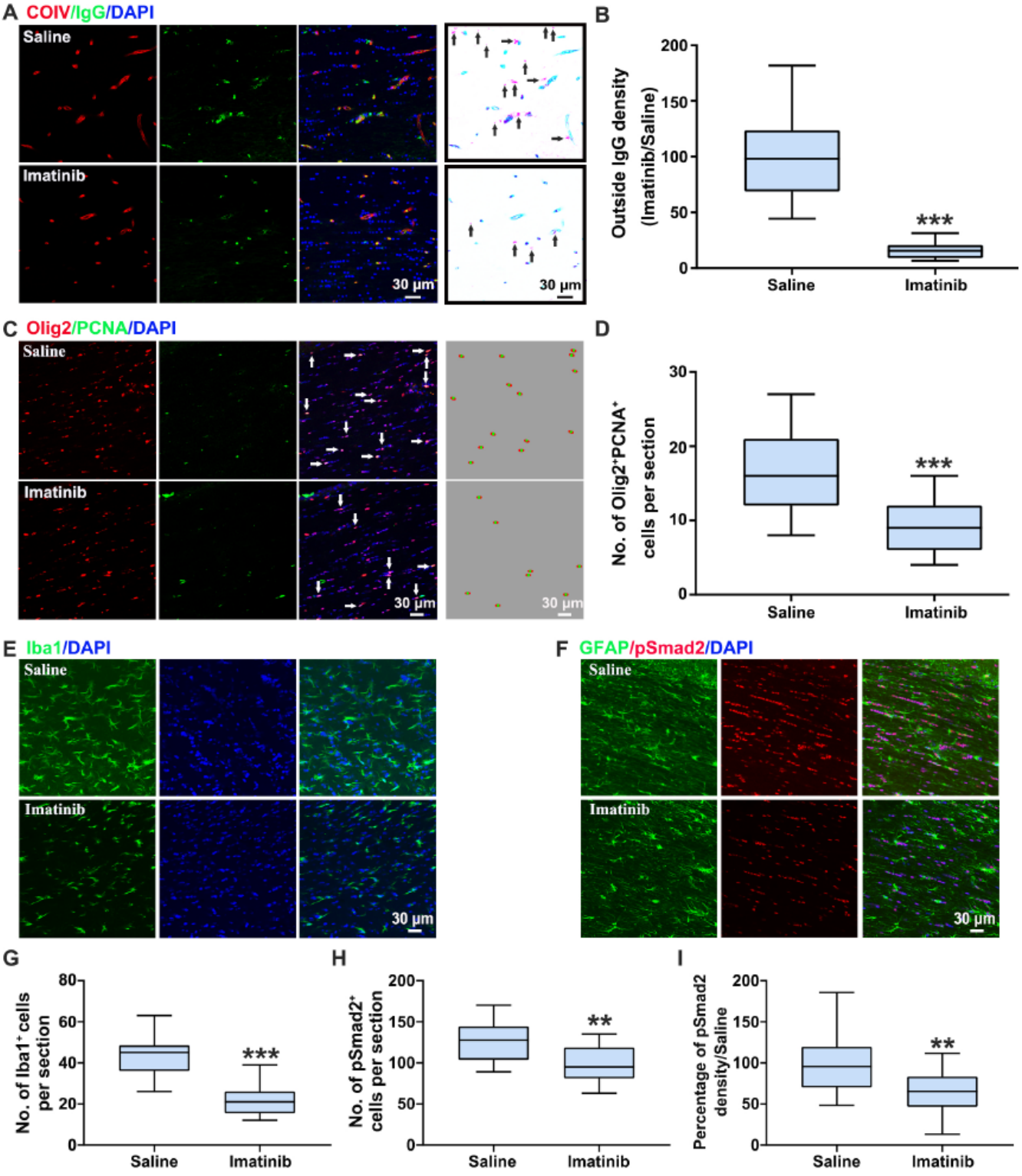

Figure 6

Extravasation of IgG is abolished after Imatinib treatment following CCH. (A) Confocal images show reduced IgG extravasation in the CC after Imatinib treatment. Schematic diagram of IgG in representative confocal microscopy image is shown in the right column. Black arrows indicate IgG accumulation outside of the vessels. (B) Quantification of outside IgG density after Imatinib treatment. (C) Confocal images show reduced proliferation of OPCs in the CC after Imatinib treatment. White arrows indicate

proliferative OPCs. Schematic diagram of the number of proliferative OPCs in representative confocal microscopy image is shown in the right column. (D) Quantification of the number of proliferative OPCs (Olig2+PCNA+) after Imatinib treatment. (E-F) Confocal images show reduced microglia activation and pSmad2 density in the CC after Imatinib treatment. (G-I) Quantification of the number of Iba+ cells and pSmad2+ cells, pSmad2 density in the CC after Imatinib treatment. n=3 per group; ***p < 0.001; compared to saline group by Student's t test, two tailed.

Supplementary Files

This is a list of supplementary files associated with this preprint. Click to download.

- supportinginformation.docx